Current-induced magnetization dynamics in two magnetic insulators separated by a normal metal

Hans Skarsvåg,[1] Gerrit E. W. Bauer,[2,3] and Arne Brataas[1]

[1]*Department of Physics, Norwegian University of Science and Technology, NO-7491 Trondheim, Norway*

[2]*Institute for Materials Research and WPI-AIMR, Tohoku University, Sendai 980-8577, Japan*

[3]*Kavli Institute of NanoScience, Delft University of Technology, 2628 CJ Delft, Netherlands*

(Received 9 May 2014; revised manuscript received 8 July 2014; published 4 August 2014)

We study the dynamics of spin valves consisting of two layers of magnetic insulators separated by a normal metal in the macrospin model. A current through the spacer generates a spin Hall current that can actuate the magnetization via the spin-transfer torque. We derive expressions for the effective Gilbert damping and the critical currents for the onset of magnetization dynamics including the effects of spin pumping that can be tested by ferromagnetic resonance experiments. The current generates an amplitude asymmetry between the in-phase and out-of-phase modes. We discuss superlattices of stacked films of metals and magnetic insulators.

DOI: 10.1103/PhysRevB.90.054401 PACS number(s): 76.50.+g, 75.30.Ds, 75.70.−i, 75.76.+j

I. INTRODUCTION

Electric currents induce spin-transfer torques in heterogeneous or textured magnetic systems [1]. In this context, magnetic insulators such as yttrium iron garnet (YIG) combined with normal-metal contacts exhibiting spin-orbit interactions, such as Pt, have recently attracted considerable interest, both experimentally [2–8] and theoretically [9–15]. Since the discovery of nonlocal exchange coupling and giant magnetoresistance in spin valves, i.e., a normal metal sandwiched between two ferromagnetic metals, these systems have been known to display rich physics. Some of these effects, such as the dynamic exchange interaction [16], should also arise when the magnetic layers are insulators. The spin Hall magnetoresistance (SMR) is predicted to be enhanced in such spin valves [10], although experimental realizations have not yet been reported. Here, we consider multilayer structures with ferromagnetic but electrically insulating (FI) layers and normal-metal (N) spacers. In-plane electric currents applied to N generate perpendicular spin currents via the spin Hall effect (SHE). When these spin currents are absorbed at the N|FI interfaces, the ensuing spin-transfer torques can induce magnetization dynamics and switching. We consider ground-state configurations in which the magnetizations are parallel or antiparallel to each other. For thin magnetic layers, even small torques can effectively modify the (Gilbert) damping, which can be observed as changes in the line width of the ferromagnetic resonance (FMR) spectra. We employ the macrospin model for the magnetization vectors that is applicable for sufficiently strong and homogeneous magnetic fields, while extensions are possible [13–15]. Our results include the calculation of effective (anti)damping resulting from in-plane charge currents in FI|N|FI trilayers, magnetic stability analysis in the current-magnetic field parameter space, and a brief analysis of the dynamics for currents above the critical value. We also consider current-induced effects in superlattices. Our paper is organized as follows. In Sec. II, we present our model for a FI|N|FI spin valve including the SHE spin-current generation and spin pumping, modeled as additional torques in the Landau-Lifshitz-Gilbert equation. We proceed to formulate the linearized magnetization dynamics and the spin accumulation in N in Sec. III. In Sec. IV, we calculate the eigenmodes and the current-controlled effective Gilbert damping and determine the critical currents at which the magnetic precession becomes unstable. We discuss the current-induced dynamics of $\cdots|\mathrm{FI}|\mathrm{N}|\mathrm{FI}|\mathrm{N}|\cdots$ superlattices in Sec. V. Finally, we summarize our conclusions and provide an outlook in Sec. VI.

II. MODEL

FI1|N|FI2 denotes the heterostructure composed of a N layer sandwiched between two layers of FIs (see Fig. 1). We denote the thicknesses of FI1, N, and FI2 by d_1, d_N, and d_2, respectively. We adopt a macrospin model of spatially constant magnetization $\mathbf{M}_i$ in each layer. The magnetization dynamics of the two layers are described by the coupled Landau-Lifshitz-Gilbert-Slonczewski (LLGS) equations:

$$\dot{\mathbf{M}}_i = -\gamma \mathbf{M}_i \times \left(\mathbf{H}_{\mathrm{eff},i} + \frac{J}{d_i M_{S,i}} \mathbf{M}_j \right) + \alpha_i \mathbf{M}_i \times \dot{\mathbf{M}}_i + \boldsymbol{\tau}_i^{\mathrm{DSP}} + \boldsymbol{\tau}_i^{\mathrm{ISP}} + \boldsymbol{\tau}_i^{\mathrm{SH}}, \tag{1}$$

where $\mathbf{M}_i$ is the unit vector in the direction of the magnetization in the left/right layer with indices $i = 1,2$; $M_{S,i}$ is the saturation magnetization; γ is the gyromagnetic ratio; α_i is the Gilbert damping constant; J is the interlayer dipolar and exchange energy areal density [17], with $j = 1\,(2)$ when $i = 2$ (1); and $\mathbf{H}_{\mathrm{eff},i}$ is an effective magnetic field:

$$\mathbf{H}_{\mathrm{eff},i} = \mathbf{H}_{\mathrm{ext}} + \mathbf{H}_{\mathrm{an},i}\left(\mathbf{M}_i\right), \tag{2}$$

consisting of the external magnetic field $\mathbf{H}_{\mathrm{ext}}$ as well as the anisotropy fields $\mathbf{H}_{\mathrm{an},i}$ for the left/right layer. We distinguish direct (DSP) and indirect (ISP) spin pumping. DSP generates the spin angular momentum current $\mathbf{j}_{1(2)}^{\mathrm{DSP}}$ through the interfaces of FI1 (FI2). A positive spin current corresponds to a spin flow toward the FI from which it originates. The DSP spin current is expressed as

$$\mathbf{j}_i^{\mathrm{DSP}} = \frac{\hbar}{e} g_{\perp,i} \mathbf{M}_i \times \dot{\mathbf{M}}_i, \tag{3}$$

where $g_{\perp,i}$ is the real part of the spin-mixing conductance of the N|FI1 (FI2) interface per unit area for $i = 1$ (2), respectively, and $-e$ is the electron charge. This angular momentum loss causes a damping torque (here and below in cgs units):

$$\boldsymbol{\tau}_i^{\mathrm{DSP}} = \frac{\gamma \hbar^2 g_{\perp,i}}{2e^2 M_{S,i} d_i} \mathbf{M}_i \times \dot{\mathbf{M}}_i. \tag{4}$$

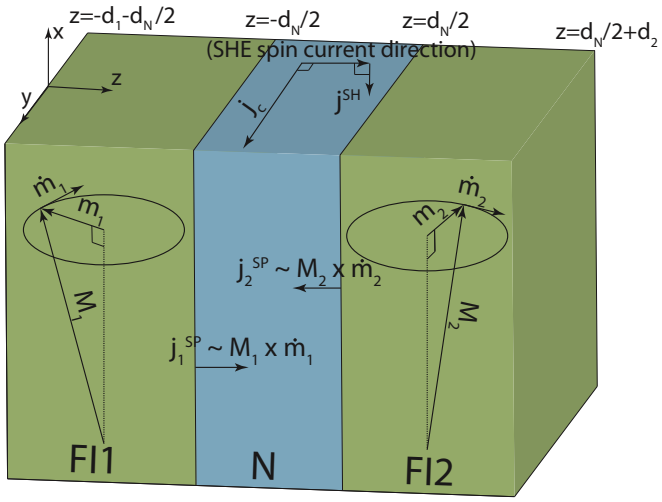

FIG. 1. (Color online) Spin valve of ferromagnetic insulators (FIs) sandwiching a normal metal (N). The magnetizations $\mathbf{M}_1$ and $\mathbf{M}_2$ are collinear at equilibrium, i.e., parallel or antiparallel. A spin-Hall-induced spin current flows in the z direction and is polarized along x.

In ballistic systems, the spin current emitted by the neighboring layer is directly absorbed and generates an indirect spin torque on the opposing layer [16]:

$$\boldsymbol{\tau}_{i,\mathrm{ball}}^{\mathrm{ISP}} = -\frac{\gamma\hbar^2 g_{\perp,i}}{2e^2 M_{S,i} d_i}\mathbf{M}_i \times \dot{\mathbf{M}}_i. \tag{5}$$

In the presence of an interface or bulk disorder, the transport is diffuse, and the ISP is

$$\boldsymbol{\tau}_i^{\mathrm{ISP}} = -\frac{\gamma\hbar}{2e^2 M_{S,i} d_i} g_{\perp,i}\mathbf{M}_i \times [\mathbf{M}_i \times \boldsymbol{\mu}^{\mathrm{SP}}(z_i)], \tag{6}$$

where $\boldsymbol{\mu}^{\mathrm{SP}}(z_i)$ is the spin pumping contribution to the spin accumulation (difference in chemical potentials) at the interface in units of energy, with $z_i \equiv \mp d_{\mathrm{N}}/2$ for $i = 1,2$. $\boldsymbol{\mu}^{\mathrm{SP}}$ is the solution of the spin-diffusion equation in N as discussed below.

Due to the SHE, an in-plane dc charge current produces a transverse spin current that interacts with the FI|N interfaces. Focusing on the diffusive regime, the charge current density $\mathbf{j}_{\mathrm{c}}$ as well as the spin $\mathbf{j}_k^{\mathrm{SH}}$ current density in the k direction, where $\mathbf{j}_k^{\mathrm{SH}}/|\mathbf{j}_k^{\mathrm{SH}}|$ is the spin polarization unit vector, can be written in terms of a symmetric linear response matrix [10]:

$$\begin{pmatrix} \mathbf{j}_{\mathrm{c}} \\ \mathbf{j}_x^{\mathrm{SH}} \\ \mathbf{j}_y^{\mathrm{SH}} \\ \mathbf{j}_z^{\mathrm{SH}} \end{pmatrix} = \sigma \begin{pmatrix} 1 & \Theta_{\mathrm{SH}}\hat{\mathbf{x}}\times & \Theta_{\mathrm{SH}}\hat{\mathbf{y}}\times & \Theta_{\mathrm{SH}}\hat{\mathbf{z}}\times \\ \Theta_{\mathrm{SH}}\hat{\mathbf{x}}\times & 1 & 0 & 0 \\ \Theta_{\mathrm{SH}}\hat{\mathbf{y}}\times & 0 & 1 & 0 \\ \Theta_{\mathrm{SH}}\hat{\mathbf{z}}\times & 0 & 0 & 1 \end{pmatrix} \times \begin{pmatrix} -\nabla\mu_c/e \\ -\nabla\mu_x^{\mathrm{SH}}/(2e) \\ -\nabla\mu_y^{\mathrm{SH}}/(2e) \\ -\nabla\mu_z^{\mathrm{SH}}/(2e) \end{pmatrix}, \tag{7}$$

where Θ^{SH} is the spin Hall angle, σ is the electrical conductivity, and μ_c is the charge chemical potential. $\boldsymbol{\mu}^{\mathrm{SH}} = (\mu_x^{\mathrm{SH}}, \mu_y^{\mathrm{SH}}, \mu_z^{\mathrm{SH}})$ is the spin accumulation induced by reflection of the spin currents at the interfaces. The spin-transfer torques $\boldsymbol{\tau}_i^{\mathrm{SH}}$ at the FI interfaces ($i = 1,2$) are then expressed as

$$\boldsymbol{\tau}_i^{\mathrm{SH}} = -\frac{\gamma\hbar}{2e^2 M_{S,i} d_i} g_{\perp,i}\mathbf{M}_i \times [\mathbf{M}_i \times \boldsymbol{\mu}^{\mathrm{SH}}(z_i)]. \tag{8}$$

The polarization of $\boldsymbol{\mu}^{\mathrm{SH}}$ and thereby $\boldsymbol{\tau}_i^{\mathrm{SH}}$ can be controlled by the charge-current direction. In the following sections, we assume that the shape anisotropy and exchange coupling favor parallel or antiparallel equilibrium orientations of $\mathbf{M}_1$ and $\mathbf{M}_2$. For small current levels, the torques normal to the magnetization induce tilts from their equilibrium directions, and at sufficiently large currents, they trigger complicated dynamics, while torques directed along the equilibrium magnetization modify the effective damping and induce magnetization reversal. Here, we focus on the latter configuration, in which the spin accumulation in N is collinear to the equilibrium magnetizations.

In the following equations, we take the thickness, saturation magnetization, Gilbert damping, and spin-mixing conductance to be equal in layers FI1 and FI2, with an out-of-plane hard axis and an in-plane internal field:

$$\mathbf{H}_{\mathrm{eff},1} = \frac{\omega_H}{\gamma}\hat{\mathbf{x}} - \frac{\omega_M}{\gamma}(\mathbf{M}_1)_z\hat{\mathbf{z}}, \tag{9a}$$

$$\mathbf{H}_{\mathrm{eff},2} = s\frac{\omega_H}{\gamma}\hat{\mathbf{x}} - \frac{\omega_M}{\gamma}(\mathbf{M}_2)_z\hat{\mathbf{z}}, \tag{9b}$$

with $\omega_H = \gamma[H_{\mathrm{ext}} + (H_{\mathrm{an},i})_x]$ and $\omega_M = 4\pi\gamma M_S$. Pure dipolar interlayer coupling with $J < 0$ favors an antiparallel ground-state configuration, while the exchange coupling oscillates as a function of d_N.

III. SPIN-TRANSFER TORQUES

The spin-pumping and spin-transfer torques $\boldsymbol{\tau}_i^{\mathrm{DSP}}$ and $\boldsymbol{\tau}_i^{\mathrm{ISP}}$ [Eqs. (4) and (6)] cause dynamic coupling between the two magnetizations. To leading order, these torques can be treated separately. We now derive expressions for disordered systems that support spin accumulations $\boldsymbol{\mu}^{\mathrm{X}}(z)$ (X = SH,SP) governed by the spin-diffusion equation:

$$\dot{\boldsymbol{\mu}}^{\mathrm{X}} = D\partial_z^2\boldsymbol{\mu}^{\mathrm{X}} - \frac{\boldsymbol{\mu}^{\mathrm{X}}}{\tau_{\mathrm{sf}}}. \tag{10}$$

Here, D is the diffusion constant, and τ_{sf} is the spin-flip relaxation time. The diffuse spin current in the z direction related to this spin accumulation follows Eq. (7):

$$\mathbf{j}^{\mathrm{X}} = -\frac{\sigma}{2e}\frac{\partial\boldsymbol{\mu}^{\mathrm{X}}}{\partial z}, \tag{11}$$

where σ is the conductivity of N.

A. Spin-pumping-induced torques

The total spin current into an FI is the sum of the spin-transfer and spin-pumping currents. Disregarding interface spin-flip scattering, the boundary conditions for the left/right

layer are

$$-\frac{1}{e}g_\perp \mathbf{M}_i \times [\mathbf{M}_i \times \boldsymbol{\mu}^{\rm SP}(z_i)] + \mathbf{j}_i^{\rm DSP} = \mp \mathbf{j}^{\rm SP}(z_i). \quad (12)$$

The minus (plus) sign on the right-hand side is due to the opposite flow direction of the spin currents at the left (right) interface. We expand the magnetization direction around the equilibrium configuration as

$$\mathbf{M}_1 = \hat{\mathbf{x}} + \mathbf{m}_1, \quad (13a)$$

$$\mathbf{M}_2 = s\hat{\mathbf{x}} + \mathbf{m}_2, \quad (13b)$$

as long as $|\mathbf{m}_i| \ll |\mathbf{M}_i|$ or $\mathbf{m}_i \cdot \mathbf{M}_i = \mathcal{O}(|\mathbf{m}_i|^2)$. The parameter $s = 1$ when the equilibrium configuration is parallel; $s = -1$ when it is antiparallel. The FMR frequency is usually much smaller than the diffuse electron traversal rate $D/d_{\rm N}^2$ and spin-flip relaxation $1/\tau_{\rm sf}$ rate; thus, retardation of the spin flow may be disregarded. In the steady state, the left-hand side of Eq. (10) vanishes. We solve Eq. (10) for the adiabatic magnetization dynamics with boundary conditions (12) to obtain the spin accumulation:

$$\boldsymbol{\mu}^{\rm SP} = -\frac{\hbar}{2}\hat{\mathbf{x}} \times [(\dot{\mathbf{m}}_1 + s\dot{\mathbf{m}}_2)\Gamma_1(z) - (\dot{\mathbf{m}}_1 - s\dot{\mathbf{m}}_2)\Gamma_2(z)], \quad (14)$$

where $l_{\rm sf} = \sqrt{D\tau_{\rm sf}}$ is the spin-diffusion length and

$$\Gamma_1(z) \equiv \frac{\cosh(z/l_{\rm sf})}{\cosh(d_{\rm N}/2l_{\rm sf}) + \sigma \sinh(d_{\rm N}/2l_{\rm sf})/2g_\perp l_{\rm sf}}, \quad (15a)$$

$$\Gamma_2(z) \equiv \frac{\sinh(z/l_{\rm sf})}{\sinh(d_{\rm N}/2l_{\rm sf}) + \sigma \cosh(d_{\rm N}/2l_{\rm sf})/2g_\perp l_{\rm sf}}. \quad (15b)$$

The torques are

$$\boldsymbol{\tau}_i^{\rm ISP} = \frac{\gamma\hbar}{2e^2 M_S d} g_\perp \boldsymbol{\mu}^{\rm SP}(z_i). \quad (16)$$

Because the spin accumulation is generated by the dynamics of both ferromagnets, we obtain spin-pumping-induced dynamic coupling that is quenched when $d_{\rm N} \gg l_{\rm sf}$. In the limit of vanishing spin-flip scattering, the spin accumulation is spatially constant and is expressed as

$$\boldsymbol{\mu}^{\rm SP} \overset{d_{\rm N} \ll l_{\rm sf}}{\to} -\frac{\hbar}{2}\hat{\mathbf{x}} \times (\dot{\mathbf{m}}_1 + s\dot{\mathbf{m}}_2). \quad (17)$$

The corresponding diffusive torque is then a simple average of the contributions from the two spin-pumping currents, in contrast to the ballistic torque that depends only on the magnetization on the opposite side.

B. Current-induced torques

A charge current in the y direction causes a spin Hall current in the z direction that is polarized along the x direction (see Fig. 1). At the interfaces, the current induces a spin-accumulation $\boldsymbol{\mu}^{\rm SH}$ that satisfies the diffusion equation (10) and drives a spin current (dropping the index z from now on):

$$\mathbf{j}^{\rm SH} = -\frac{\sigma}{2e}\frac{\partial \boldsymbol{\mu}^{\rm SH}}{\partial z} - j_0^{\rm SH}\hat{\mathbf{x}}, \quad (18)$$

where $j_0^{\rm SH} = \Theta_{\rm SH} j_c$. Angular momentum conservation at the left and right boundaries leads to

$$-\frac{1}{e}g_\perp \mathbf{M}_i \times [\mathbf{M}_i \times \boldsymbol{\mu}^{\rm SH}(z_i)] = \mp \mathbf{j}^{\rm SH}(z_i). \quad (19)$$

When $\mathbf{M}_i \parallel \boldsymbol{\mu}^{\rm SH}$, the spin Hall current is completely reflected, and the spin current at the interface vanishes, while the absorption and torque are maximal when $\mathbf{M}_i \perp \boldsymbol{\mu}^{\rm SH}$. Spin currents and torques at the interface scale favor $\mathbf{m}_i$ for small magnetization amplitudes. Let us define a time-independent $\boldsymbol{\mu}_0^{\rm SH}$ for collinear magnetizations and spin-current polarization. For small dynamic magnetizations,

$$\boldsymbol{\mu}^{\rm SH} = \boldsymbol{\mu}_0^{\rm SH} + \delta\boldsymbol{\mu}^{\rm SH}, \quad (20)$$

where $\delta\boldsymbol{\mu}^{\rm SH} \sim \mathbf{m}_i$. The spin-Hall-induced spin accumulation leads to an (anti)damping torque in the trilayer, while contributing to the real part of the frequency in superlattices (see Sec. V).

Solving the diffusion equation (10) with boundary conditions, Eq. (19) yields

$$\boldsymbol{\mu}_0^{\rm SH} = -\frac{2el_{\rm sf}}{\sigma} j_0^{\rm SH} \frac{\sinh(z/l_{\rm sf})}{\cosh(d_{\rm N}/2l_{\rm sf})}\hat{\mathbf{x}}. \quad (21)$$

The dynamic correction

$$\delta\boldsymbol{\mu}^{\rm SH} = -\frac{1}{2}\frac{2el_{\rm sf}}{\sigma} j_0^{\rm SH} \tanh(d_{\rm N}/2l_{\rm sf}) \times [(\mathbf{m}_1 + s\mathbf{m_2})\Gamma_2(z) - (\mathbf{m}_1 - s\mathbf{m_2})\Gamma_1(z)] \quad (22)$$

generates SHE torques [Eq. (8)]:

$$\boldsymbol{\tau}_i^{\rm SH} = -\frac{\gamma\hbar}{2e^2 M_S d} g_\perp \left[\mathbf{m}_i\left(\boldsymbol{\mu}_0^{\rm SH} \cdot \hat{\mathbf{x}}\right) - \delta\boldsymbol{\mu}^{\rm SH}(z_i)\right]. \quad (23)$$

Equation (1) then reduces to four coupled linear first-order partial differential equations for $\mathbf{m}_i$.

IV. EIGENMODES AND CRITICAL CURRENTS

After linearizing Eq. (1) and Fourier transforming to the frequency domain $\dot{\mathbf{M}}_i \to i\omega\hat{\mathbf{m}}_i$, Eq. (1) becomes

$$\mathcal{M}\mathbf{v} = 0, \quad (24)$$

where $\mathbf{v}^T = (\hat{m}_{1,y}, \hat{m}_{1,z}, \hat{m}_{2,y}, \hat{m}_{2,z})$ and $\mathcal{M}$ is a 4×4 frequency-dependent matrix that can be decomposed as

$$\mathcal{M} = \mathcal{M}_0 + J\mathcal{M}_J + (\alpha + \alpha')\mathcal{M}_{\rm d} + \alpha'\mathcal{M}_{\rm SP} + j_0^{\rm SH}\mathcal{M}_{\rm SH}, \quad (25)$$

with

$$\mathcal{M}_0 = \begin{pmatrix} -i\omega & -\tilde{\omega}_H - \omega_M & 0 & 0 \\ \tilde{\omega}_H & -i\omega & 0 & 0 \\ 0 & 0 & -i\omega & -s\tilde{\omega}_H - s\omega_M \\ 0 & 0 & s\tilde{\omega}_H & -i\omega \end{pmatrix}, \quad (26a)$$

$$\mathcal{M}_{\rm d} = \begin{pmatrix} 0 & -i\omega & 0 & 0 \\ i\omega & 0 & 0 & 0 \\ 0 & 0 & 0 & -is\omega \\ 0 & 0 & is\omega & 0 \end{pmatrix}, \quad (26b)$$

$$\mathcal{M}_{\rm J} = \begin{pmatrix} 0 & 0 & 0 & \omega_x \\ 0 & 0 & -\omega_x & 0 \\ 0 & s\omega_x & 0 & 0 \\ -s\omega_x & 0 & 0 & 0 \end{pmatrix}, \tag{26c}$$

$$\mathcal{M}_{\rm ISP} = \begin{pmatrix} 0 & i\omega F' & 0 & is\omega G' \\ -i\omega F' & 0 & -is\omega G' & 0 \\ 0 & i\omega G' & 0 & is\omega F' \\ -i\omega G' & 0 & -is\omega F' & 0 \end{pmatrix}, \tag{26d}$$

$$\mathcal{M}_{\rm SH} = \begin{pmatrix} -F & 0 & -sG & 0 \\ 0 & -F & 0 & -sG \\ G & 0 & sF & 0 \\ 0 & G & 0 & sF \end{pmatrix}. \tag{26e}$$

Here, $\mathcal{M}_0$ describes dissipationless precession in the effective magnetic fields, $\mathcal{M}_{\rm d}$ arises from Gilbert damping and the direct effect of spin pumping with a renormalized damping coefficient $\tilde{\alpha} = \alpha + \alpha'$ and

$$\alpha' = \frac{\gamma\hbar^2}{2e^2 M_s d} g_\perp, \tag{27}$$

$\mathcal{M}_{\rm J}$ represents interlayer exchange coupling, $\mathcal{M}_{\rm ISP}$ represents spin-pumping-induced spin transfer, and $\mathcal{M}_{\rm SH}$ represents the spin transfer caused by the spin Hall current. The external and possible in-plane anisotropy fields are modified by the interlayer coupling, $\omega_H \to \tilde{\omega}_H = \omega_H + \omega_x$, where $\omega_x = \gamma J/(M_s d)$. The matrix elements F', G', F, and G are generalized susceptibilities extracted from Eqs. (16) and (23):

$$F' = \frac{1}{\alpha'} \frac{\partial \left(\boldsymbol{\tau}_1^{\rm ISP}\right)_y}{\partial \dot{m}_{1,z}}, \tag{28a}$$

$$G' = \frac{1}{\alpha'} \frac{\partial \left(\boldsymbol{\tau}_1^{\rm ISP}\right)_y}{\partial (s\dot{m}_{2,z})}, \tag{28b}$$

$$F = -\frac{1}{j_0^{\rm SH}} \frac{\partial \left(\boldsymbol{\tau}_1^{\rm SH}\right)_y}{\partial m_{1,y}}, \tag{28c}$$

$$G = \frac{1}{j_0^{\rm SH}} \frac{\partial \left(\boldsymbol{\tau}_1^{\rm SH}\right)_y}{\partial (s m_{2,y})}. \tag{28d}$$

The explicit expressions given in Appendix A are simplified for very thick and thin N spacers.

Thin N layer. When $d_{\rm N} \ll l_{\rm sf}$, the interlayer coupling G' due to spin pumping approaches F', the intralayer coupling:

$$G' \to F' \to \tfrac{1}{2}, \tag{29}$$

which implies that the incoming and outgoing spin currents are the same. This outcome represents the limit of strong dynamic coupling in which the additional Gilbert damping due to spin pumping vanishes when the magnetization motion is synchronized [18]. In this regime, the SHE becomes ineffective because F and G scale as $d_{\rm N}/l_{\rm sf}$. $F/G \to 2$ because F contains a contribution from both the static and the dynamic spin accumulations.

Thick N layer. In the thick-film limit, $d_{\rm N} \gg l_{\rm sf}$, the interlayer coupling vanishes as $G \to 0$ and $G' \to 0$, while

$$F' \to \frac{1}{1 + \frac{\sigma}{2g_\perp l_{\rm sf}}}, \tag{30a}$$

$$F \to \frac{\gamma\hbar}{2eM_S d} \frac{1}{1 + \frac{\sigma}{2g_\perp l_{\rm sf}}}. \tag{30b}$$

Introducing the spin conductance $G_{\rm sf} \equiv \mathcal{A}\sigma/2l_{\rm sf}$, $G_\perp = \mathcal{A}g_\perp$, and $R_{\rm tot} = (G_\perp + G_{\rm sf})^{-1}$, the total resistance of the interface and the spin active region of N. Then $F' \to R_{\rm tot}G_\perp$, represents the backflow of pumped spins. The same holds for the part of F that originates from the dynamic part of $\boldsymbol{\mu}^{\rm SH}$, while the static part approaches a constant value when $d_{\rm N}$ becomes large (see the Appendix). In this limit, the system reduces to two decoupled FI|N bilayers.

The eigenmodes of the coupled system are the solutions of $\det[\mathcal{M}(\omega_n)] = 0$ with complex eigenfrequencies ω_n. The SHE spin current induces spin accumulations with opposite polarizations at the two interfaces. In the parallel case, the torques acting on the two FIs are exerted in opposite directions. The torques then stabilize one magnetization, but destabilize the other. When the eigenfrequencies acquire a negative imaginary part, their amplitude grows exponentially in time. We define the threshold current $j_{0,\rm thr}^{\rm SH}$ by the value at which $\mathrm{Im}[\omega_n(j_{0,\rm thr}^{\rm SH})] = 0$. Because the total damping has to be overcome at the threshold, $j_{0,\rm thr}^{\rm SH} \sim \tilde{\alpha}$. We treat the damping and exchange coupling perturbatively, thereby assuming $\tilde{\alpha} \ll 1$ and $\omega_x \ll \omega_0$, where $\omega_0 = \sqrt{\tilde{\omega}_H(\tilde{\omega}_H + \omega_M)}$ is the FMR frequency. The spin Hall angle is usually much smaller than unity; thus, $j_0^{\rm SH}$ is treated as a perturbation for currents up to the order of the threshold current, implying that $|\mathrm{Im}[\omega_n(j_0^{\rm SH})]| \ll |\mathrm{Re}[\omega_n(j_0^{\rm SH})]|$.

The exchange coupling $\omega_x = \gamma J/(M_s d)$ for YIG|Pt|YIG should be weaker than that of the well-studied metallic magnetic monolayers, where it is known to become very small for $d \gtrsim 3$nm [19]. In the following sections, we assume that $\omega_x \ll \omega_M$ may be treated as a perturbation.

To treat the damping, spin pumping, spin-Hall-induced torques, and static exchange perturbatively, we introduce the smallness parameter ϵ and let $\alpha \to \epsilon\alpha$, $\alpha' \to \epsilon\alpha'$, $j_0^{\rm SH} \to \epsilon j_0^{\rm SH}$, $\omega_x \to \epsilon\omega_x$. In the following sections, a first-order perturbation is applied by linearizing in ϵ and subsequently setting $\epsilon = 1$.

We transform $\mathcal{M}$ by the matrix $\mathcal{U}$ that diagonalizes $\mathcal{M}_0$ with eigenvalues $(\omega_0, \omega_0, -\omega_0, -\omega_0)$. We then extract the part corresponding to the real eigenfrequencies, which yields the following equation:

$$\begin{vmatrix} (D)_{11} & (D)_{12} \\ (D)_{21} & (D)_{22} \end{vmatrix} = 0, \tag{31}$$

where $D = \mathcal{U}^{-1}\mathcal{M}\mathcal{U}$. We thus reduce the fourth-order secular equation in ω to a second-order expression. To the first order, we find for the parallel ($s = 1$) case,

$$\omega^{\rm P} = \tilde{\omega}_0 + i\frac{\alpha_{\rm eff}^{\rm P}}{2}(2\tilde{\omega}_H + \omega_M), \tag{32}$$

where we introduced a current-controlled effective Gilbert damping:

$$\alpha_{\rm eff}^{\rm P} = \alpha + \alpha'(1-F') \pm \sqrt{\left(\alpha' G' - i\frac{\omega_x}{\omega_0}\right)^2 + \frac{4(F^2-G^2)\left(j_0^{\rm SH}\right)^2}{(2\tilde{\omega}_H+\omega_M)^2}}. \quad (33)$$

The imaginary part of the square root in Eq. (33) causes a first-order real frequency shift that we may disregard, i.e., $\mathrm{Re}[\omega^{\rm P}] \approx \tilde{\omega}_0 \approx \omega_0$. We thus find two modes with nearly the same frequencies but different effective broadenings.

The critical current $j_{0,\rm thr}^{\rm SH,P}$ is now determined by requiring that $\alpha_{\rm eff}^{\rm P}$ vanish, leading to

$$j_{0,\rm thr}^{\rm SH,P} = \pm \frac{\sqrt{[\alpha+\alpha'(1-F')]^2-(\alpha' G')^2}}{2\sqrt{F^2-G^2}} \times \sqrt{1+\left(\frac{\omega_x/\omega_0}{\alpha+\alpha'(1-F')}\right)^2}(2\tilde{\omega}_H+\omega_M), \quad (34)$$

while the critical charge current is $j_{\rm c,thr}^{\rm P} = j_{0,\rm thr}^{\rm S,P}/\Theta_{\rm SH}$. Spin pumping and spin flip dissipate energy, leading to a higher threshold current, which is reflected by $1-F' \geqslant G'$. The reactive part of the SHE-induced torque (G) suppresses the effect of the applied current and thereby increases the critical current as well. The static exchange couples $\mathbf{M}_1$ and $\mathbf{M}_2$, hence increasing $j_{0,\rm thr}^{\rm SH,P}$. The critical spin current decreases monotonically with increasing $d_{\rm N}/l_{\rm sf}$, implying that the spin valve (with parallel magnetization) has a larger threshold current than the FI|N bilayer (with thick $d_{\rm N}$).

Analogous to the parallel case, we find two eigenmodes for the antiparallel case ($s=-1$), with eigenfrequencies

$$\omega^{\rm AP} = \omega_0 + \left(\pm\frac{-\omega_x}{2\omega_0} + i\frac{\alpha_{\rm eff}^{\rm AP}}{2}\right)(2\tilde{\omega}_H+\omega_M) \quad (35)$$

and corresponding effective Gilbert damping parameters

$$\alpha_{\rm eff}^{\rm AP} = \alpha + \alpha'(1-F') \pm \alpha' G' \frac{\omega_M}{2\tilde{\omega}_H+\omega_M} + \frac{2}{2\tilde{\omega}_H+\omega_M} F j_0^{\rm SH}, \quad (36)$$

which depend on the magnetic configuration because the dynamic exchange coupling differs, while the resonance frequency is affected by the static coupling. In the AP configurations, the spin Hall current acts with the same sign on both layers due to the increase/decrease in damping on both sides depending on the applied current direction. The corresponding threshold current is expressed as

$$j_{0,\rm thr}^{\rm SH,AP} = -\frac{[\alpha+\alpha'(1-F')](2\tilde{\omega}_H+\omega_M)-\alpha' G'\omega_M}{2F}, \quad (37)$$

with $j_{c,\rm thr}^{\rm SH,AP} = j_{0,\rm thr}^{\rm SH,AP}/\Theta_{\rm SH}$. Again, the threshold for current-induced excitation is increased by the spin pumping.

To zeroth order in the smallness parameter ϵ, we find that the eigenvectors for the parallel configuration take the form $\mathbf{v}^{\rm P} = (\mathbf{u}, \beta\mathbf{u})^T$, where $\mathbf{u}$ is the two-component vector

$$\mathbf{u} = \begin{pmatrix} i\sqrt{1+\omega_M/\tilde{\omega}_H} \\ 1 \end{pmatrix}. \quad (38)$$

The imbalance in the amplitudes of both layers is parameterized by

$$\beta = \frac{2j_0^{\rm SH}F \mp \sqrt{4(F^2-G^2)\left(j_0^{\rm SH}\right)^2 + \left(\alpha' G' - i\frac{\omega_x}{\omega_0}\right)^2(2\tilde{\omega}_H+\omega_M)^2}}{-2j_0^{\rm SH}G + \left(\alpha' G' - i\frac{\omega_x}{\omega_0}\right)(2\tilde{\omega}_H+\omega_M)}, \quad (39)$$

where $\mp$ corresponds to $\pm$ in Eq. (32). For the symmetric case, the applied current favors out-of-phase oscillations. It can be demonstrated that in the limit of large currents and low spin-memory loss, the corresponding amplitude difference is $\beta=-1$, with $j_0^{\rm SH}=0$, and an interlayer coupling dominated by either dynamic or static exchange $\beta=\mp 1$, which correspond to an optical mode and an acoustic mode, respectively. We use the labels "acoustic" and "optic" even though the phase difference is not precisely 0 or π due to the static exchange interaction. Note that $\beta(-j_0^{\rm SH}) = 1/\beta(j_0^{\rm SH})$ is required by symmetry; inverting the current direction is equivalent to interchanging FI1 and FI2. For $\omega_x=0$, $\beta(j_0^{\rm SH})$ is a pole or node depending on the current direction for the acoustic mode in which the magnetization in one layer vanishes. Above this current, β change signs, and both modes have a phase difference of π (see Fig. 2). The critical current lies above the current corresponding to the node at which the acoustic mode becomes unstable. The ballistic model also supports acoustic and optical modes [16], with the optical mode being more efficiently damped.

In the antiparallel case, acoustic and optical modes are characterized by amplitudes

$$\mathbf{v}_{\rm A}^{\rm AP} = \begin{pmatrix} i\frac{\omega_0}{\tilde{\omega}_H} \\ 1 \\ i\frac{\omega_0}{\tilde{\omega}_H} \\ -1 \end{pmatrix}, \quad \mathbf{v}_{\rm O}^{\rm AP} = \begin{pmatrix} i\frac{\omega_0}{\tilde{\omega}_H} \\ 1 \\ -i\frac{\omega_0}{\tilde{\omega}_H} \\ 1 \end{pmatrix}, \quad (40)$$

where the optical (acoustic) mode corresponds to the plus (minus) sign in Eq. (35) (see Fig. 3). The labels optical and acoustic are kept because of the difference in effective damping; a 180° rotation about the y axis of FI2 maps these modes to the corresponding modes for the parallel case.

When the composition of the spin valve is slightly asymmetric, the dynamics of the two layers can still be synchronized by the static and dynamic coupling. However, at some critical detuning $\Delta\omega = \omega_2 - \omega_1$, this technique no longer works, as illustrated by the eigenfrequencies for the asymmetric spin valve in Fig. 4. Here, we employ YIG|Pt|YIG parameters but tune the FMR frequency of the right YIG layer. In practice, the

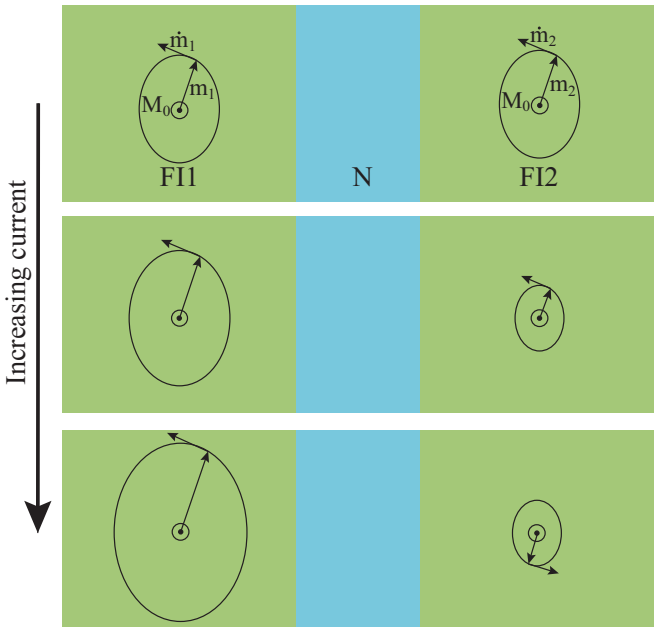

FIG. 2. (Color online) The acoustic mode for the parallel case and different applied currents, ranging from zero to just below the critical current. For large currents the oscillations of the two FIs become out of phase.

tuning can be achieved by varying the direction of the applied magnetic field [18]. When the FMR frequencies of the two layers are sufficiently close, the precessional motions in the two layers lock onto each other. The asymmetry introduced by higher currents is observed to suppress the synchronization.

The nonlinear large-angle precession that occurs for currents above the threshold is not amenable to analytical treatments; however, numerical calculations can provide some insights. Because the dissipation of YIG is very low, the number of oscillations required to achieve a noticeable change in the precession angle is very large. To speed up the calculations and make the results more readable we rescale both $g_\perp$ and α by a factor $0.005/\alpha$; in this way the effective

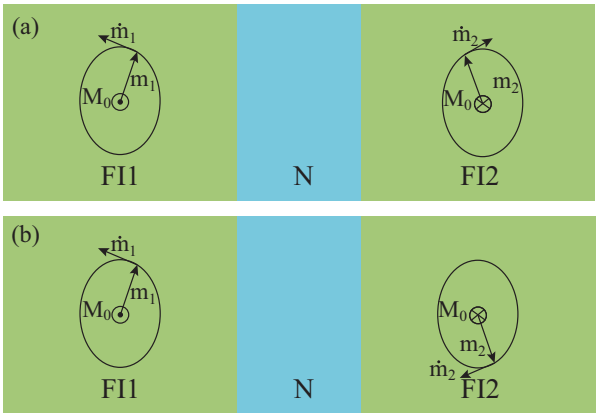

FIG. 3. (Color online) The eigenmodes of the antiparallel configuration. (a) and (b) are the acoustic and optical modes described by Eq. (40), respectively. For the acoustic (optical) mode the in-plane (out-of-plane) component is equal in the two layers but the out-of-plane (in-plane) components oppose each other.

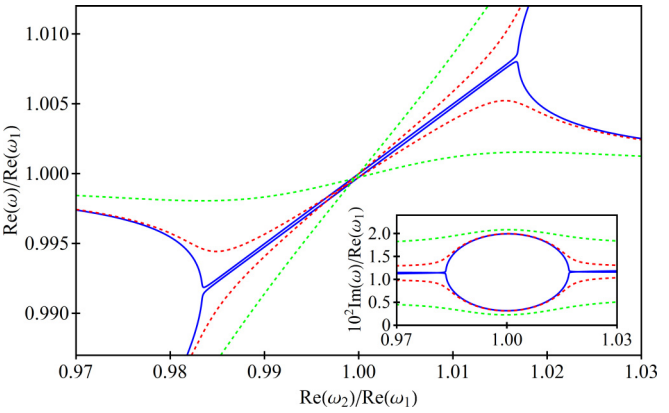

FIG. 4. (Color online) The lowest resonance frequencies of a parallel FI1|N|FI2 spin valve calculated for the parameters in Table I as a function of the detuning of the FMR frequencies of the individual layers and for different currents $j_0^{\rm SH}/j_{0,\rm thr}^{\rm SH} = 0\%, 10\%, 50\%$, represented by the solid blue, red dashed, and green dashed lines, respectively. At zero applied current the two magnetizations move in phase when detuning is small. The current suppresses synchronization almost completely when reaching the threshold value. The inset shows the corresponding broadenings.

damping is rescaled. Figure 5 shows the components of the magnetization in the two layers as a function of time when a large current is switched on for an initially parallel magnetization along x with a slight canting of $M_{i,y} = 0.01$ for $i = 1,2$. We apply a current $j_0^{\rm SH}/j_{0,\rm thr}^{\rm P,SH} = 110\%$ at $t = 0$. For $5T \lesssim t < 40T$, where $T = 2\pi/\omega_0$, the precession is out of phase, and the amplitude gradually increases. At $t = 40T$, the applied current is ramped up to $j_0^{\rm SH}/j_{0,\rm thr}^{\rm P,SH} = 130\%$. At $t \sim 60T$, the precession angle is no longer small, and our previous perturbative treatment breaks down. However, we can understand that the right layer precesses with a large angle, while the left layer stays close to the initial equilibrium from the opposite direction of the interface spin accumulations $\boldsymbol{\mu}_0^{\rm SH}$.

The macrospin model is a good approximation only in the presence of sufficiently strong applied magnetic fields that stabilize single-domain states. This might not be the case in the antiparallel configuration, and results should be viewed with some caution. Spin waves have a wave-number-dependent

TABLE I. Material parameters and sample dimensions used in the numerical calculations.

Constant	Value	Units
$g_\perp$	3.4×10^{15}[a]	$\mathrm{cm}^{-2}\, e^2/h$
σ	5.4×10^{17}[b]	s^{-1}
$4\pi M_S$	1750[c]	G
$H_{\rm int}$	$0.2 \times 4\pi M_S$	G
α	3×10^{-4}[c]	
$l_{\rm sf}$	10	nm
d_1, d_N, d_2	10, 5, 10	nm

[a]Reference [20].
[b]Reference [21].
[c]Reference [22].

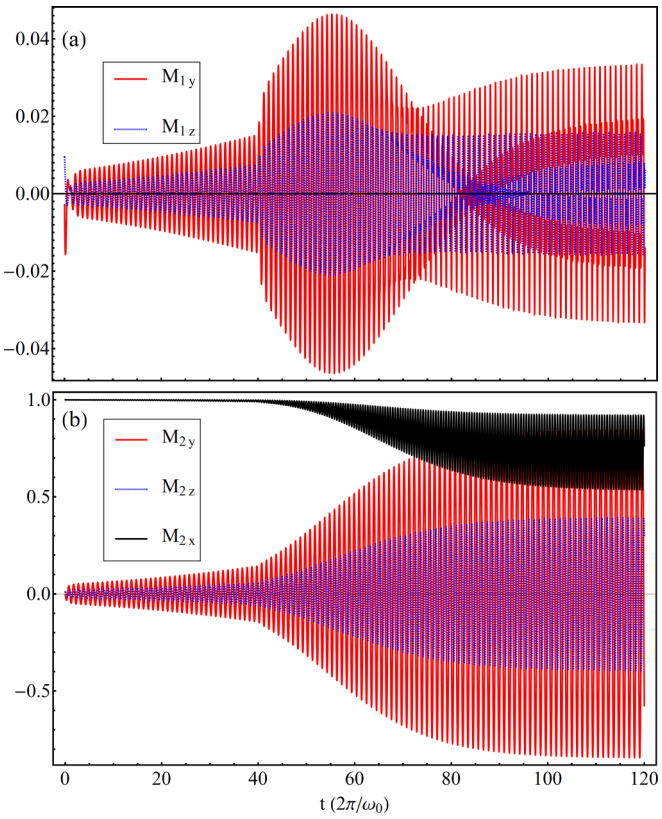

FIG. 5. (Color online) Magnetization dynamics for the parallel configuration and currents above the threshold. The magnetization in the (a) left and (b) right layers as a function of time in units of $T = 2\pi/\omega_0$. The effective damping is rescaled by letting $g_\perp \to g_\perp 0.005/\alpha$ and $\alpha \to \alpha\, 0.005/\alpha$. The numerical calculation was carried out by a fourth-order Runge-Kutta method with a step size $\Delta t = T/50$.

damping enhancement [13], which implies that the dynamic coupling in spin valves should be mode dependent [23], which cannot be treated by our model. In the nonlinear regime and FIs with dimensions exceeding the exchange length $l_{\rm ex}$ ($\sim$17 nm for YIG), the energy separation between the modes may be coupled by the large-angle dynamics, increasing dissipation and reducing the oscillation amplitude [24], which again is outside the scope of the present study.

V. SUPERLATTICES

A periodic stack of FIs coupled through Ns supports spin-wave excitations propagating in the perpendicular direction. The coupling between layers is described by Eq. (24); however, each FI is coupled through the N layers to two neighboring layers. The primitive unit cell of the superlattice with collinear magnetization is the FI|N bilayer for the collinear configuration and two bilayers in the locally antiparallel configuration, or "synthetic antiferromagnet." We introduce the layer index $i \in \mathbb{Z}$ for the local magnetization with equal (normalized) modulus

$$\mathbf{M}_i = s_i \hat{\mathbf{x}} + \mathbf{m}_i, \tag{41}$$

where $s_i = 1$ for the parallel ground state and $s_i = (-1)^i$ for the antiparallel ground state. We can linearize again the equations of motion with respect to the small parameters $\mathbf{m}_i$. For long-wavelength excitations the local magnetization for the parallel configuration, as well as the staggered field for an antiferromagnetic ordering, can be treated in the continuum limit. Denoting the total thickness of a unit cell $b = d_{\rm N} + d_{\rm FI}$, we find for the parallel case ($s_i = 1$)

$$\partial_t \mathbf{m} = \hat{\mathbf{x}} \times \{\omega_H \mathbf{m} + \omega_M m_z \hat{\mathbf{z}} + [\alpha + 2\alpha'(1 - F' - G')]\partial_t \mathbf{m} - \alpha' G'^2 \partial_{t,zz} \mathbf{m} - \omega_x b^2 \partial_{zz} \mathbf{m} + 2 j_0^{\rm SH} G b \partial_z \hat{\mathbf{x}} \times \mathbf{m}\}. \tag{42}$$

For $\mathbf{m} = \mathbf{m}_0 e^{i(\omega t - k_z z)}$, the linearized dispersion relation is

$$\omega = \sqrt{\omega_H(\omega_H + \omega_M)} + \frac{1}{2}(2\omega_H + \omega_M)\frac{\omega_x}{\omega_0} b^2 k_z^2 - 2 j_0^{\rm SH} G b k_z + i\frac{1}{2}(2\omega_H + \omega_M)\left[\alpha + 2\alpha'(1 - F' - G') + \alpha' G' k_z^2 b^2\right]. \tag{43}$$

The applied current thus adds a term that is linear in k_z to the real part of the frequency. The direct effect of the SHE now vanishes because the torques on both sides of any FI cancel. However, when $\mathbf{m}_0 \neq \mathbf{0}$, a net spin current flows normal to the stack, which affects the dispersion. In the ferromagnetic layers, this phenomenon is equivalent to a pure strain field on the magnetization and is therefore nondissipative. While generating $j_0^{\rm SH}$ causes Ohmic losses, the magnetization dynamics in this limit do not add to the energy dissipation, explaining the contribution to $\mathrm{Re}\,\omega$. In this regime, there are no external current-induced contributions or instabilities.

Synthetic antiferromagnets with Pt spacers might not be so easy to realize experimentally since, as noted above, the nonlocal exchange coupling is believed to be weak. In this configuration the unit cell is doubled as is the number of variables in the equation of motion. Determining the coupling coefficients from Eq. (26) is straightforward but cumbersome and is not presented here. Naively, one could expect that the SHE-induced torque would act quite differently in synthetic antiferromagnets. The SHE acts in a symmetric manner on the FI($\uparrow$)|N|FI($\downarrow$) system, stabilizing or destabilizing both layers simultaneously. However, similar to the ferromagnetic superlattice, the direct SHE cancels also in the synthetic antiferromagnet: each FI is sandwiched by Ns, with spin accumulations of opposite sign on the left and right sides of the interfaces, leading to the same cancellation as above.

We can also envision a multilayer in which individual metallic layers can be contacted separately and independently. N|FI|N structures have been predicted to display a magnon drag effect through the ferromagnetic film [25], i.e., a current in one layer induces an emf in the other one. A drag effect also exists in our macrospin model: if we induce dynamics by a current in one layer by the spin Hall effect, the spin pumping and inverse spin Hall effect generate a current in the other layer, but only above a current threshold.

With separate contacts to the layers one may drive opposite currents through neighboring films. In that case, the spin current absorbed by a ferromagnetic layer is approximately twice as large as that found for the FI|N bilayer and of opposite sign for neighboring magnetic layers, thereby reducing the

critical currents needed to excite the parallel configuration. Such a staggered current distribution can also stabilize an antiparallel order even in the absence of static exchange couplings. When competing with an applied magnetic field, the current-induced forces should lead to intricate dynamics. An alternative to the staggered current distribution would be structures with metals supporting spin Hall angles of opposite sign, such as Pt and Ta [26]. When grown in the alternating fashion $\cdots$N1|FI|N2|FI|N1$\cdots$, a uniform charge current generates a staggered spin Hall current distribution that can be used to force a synthetic antiferromagnetic order on the superlattice.

VI. CONCLUSIONS

We study current-induced magnetization dynamics in spin valves and superlattices consisting of insulating magnets separated by metallic spacers with the spin Hall effect. The current-induced torques experienced by the two magnetic layers in an FI(↑)|N| FI(↑) spin valve caused by the spin Hall effect are opposite in sign. A charge current in N normal to the magnetization leads to a damping and an antidamping, stabilizing one and destabilizing the other magnetization. We calculate the magnetization dynamics when the two layers are exchange coupled and in the presence of the dynamic exchange coupling induced by spin pumping. In an antiparallel configuration FI(↑)|N|FI(↓) the interlayer couplings play a minor role in the current-induced effects. The threshold currents at which self-oscillation occurs are higher for parallel than for antiparallel spin valves. We predict interesting current-induced effects for superlattices and multilayers in which the metallic spacer layers can be individually contacted or have spin Hall angles with opposite sign, such as current-induced synthetic ferromagnetic order.

ACKNOWLEDGMENTS

H.S. and A.B. acknowledge support from the Research Council of Norway, Project No. 216700. This work was supported by KAKENHI (Grants-in-Aid for Scientific Research No. 25247056 and No. 25220910), FOM (Stichting voor Fundamenteel Onderzoek der Materie), the ICC-IMR, the EU-RTN Spinicur, EU-FET Grant No. InSpin 612759, and DFG Priority Program 1538 "Spin-Caloric Transport" (BA 2954/1).

APPENDIX A: MATRIX ELEMENTS

Here, we derive the response coefficients F, G, F', and G', which determine the torques, depending on the properties of the normal metal. Let us first discuss the coefficients related to the torques induced by the SHE. The functions F and G are extracted from the derivatives of Eq. (23) with respect to the transverse components of the dynamic magnetizations $\mathbf{m}_i$. F governs the SHE-induced torque in one layer due to displaced magnetization in the same layer and can be computed as

$$\frac{\partial\left(\boldsymbol{\tau}_1^{\mathrm{SH}}\right)_y}{\partial m_{1,y}} = \frac{\partial\left(\boldsymbol{\tau}_1^{\mathrm{SH}}\right)_z}{\partial m_{1,z}} = -\frac{\partial\left(\boldsymbol{\tau}_2^{\mathrm{SH}}\right)_y}{\partial(s m_{2,y})} = -\frac{\partial\left(\boldsymbol{\tau}_2^{\mathrm{SH}}\right)_z}{\partial(s m_{2,z})} = -F j_0^{\mathrm{SH}}. \tag{A1}$$

Thus,

$$F = \frac{\gamma\hbar}{2e^2 M_S d} g_\perp \frac{2el_{\mathrm{sf}}}{\sigma} \tanh(d_{\mathrm{N}}/2l_{\mathrm{sf}}) \times \left[1 - \frac{1}{2}\Gamma_1\left(d_{\mathrm{N}}/2\right) - \frac{1}{2}\Gamma_2\left(d_{\mathrm{N}}/2\right)\right]. \tag{A2}$$

Similarly, we can identify G, which governs the cross-correlation of the SHE-induced torque in one layer arising from a displaced magnetization in the other layer, from

$$\frac{\partial\left(\boldsymbol{\tau}_1^{\mathrm{SH}}\right)_y}{\partial(s m_{2,y})} = \frac{\partial\left(\boldsymbol{\tau}_1^{\mathrm{SH}}\right)_z}{\partial(s m_{2,z})} = -\frac{\partial\left(\boldsymbol{\tau}_2^{\mathrm{SH}}\right)_y}{\partial m_{1,y}} = -\frac{\partial\left(\boldsymbol{\tau}_2^{\mathrm{SH}}\right)_z}{\partial m_{1,z}} = G j_0^{\mathrm{SH}}. \tag{A3}$$

Thus,

$$G = \frac{\gamma\hbar}{2e^2 M_S d} g_\perp \frac{2el_{\mathrm{sf}}}{\sigma} \tanh(d_{\mathrm{N}}/2l_{\mathrm{sf}}) \times \frac{1}{2}\left[\Gamma_1\left(d_{\mathrm{N}}/2\right) - \Gamma_2\left(d_{\mathrm{N}}/2\right)\right]. \tag{A4}$$

Torques generated by spin pumping contain terms of the form $\hat{\mathbf{x}} \times \mathbf{m}_i$ and couple the y and z components of the magnetization dynamics. We find

$$\frac{\partial\left(\boldsymbol{\tau}_1^{\mathrm{ISP}}\right)_y}{\partial \dot{m}_{1,z}} = -\frac{\partial\left(\boldsymbol{\tau}_1^{\mathrm{ISP}}\right)_z}{\partial \dot{m}_{1,y}} = \frac{\partial\left(\boldsymbol{\tau}_2^{\mathrm{ISP}}\right)_y}{\partial(s\dot{m}_{2,z})} = -\frac{\partial\left(\boldsymbol{\tau}_2^{\mathrm{ISP}}\right)_z}{\partial(s\dot{m}_{2,y})} = F'\alpha', \tag{A5}$$

where

$$2F' = \Gamma_1\left(d_{\mathrm{N}}/2\right) + \Gamma_2\left(d_{\mathrm{N}}/2\right). \tag{A6}$$

Similarly,

$$\frac{\partial\left(\boldsymbol{\tau}_1^{\mathrm{ISP}}\right)_y}{\partial(s\dot{m}_{2,z})} = -\frac{\partial\left(\boldsymbol{\tau}_1^{\mathrm{ISP}}\right)_z}{\partial(s\dot{m}_{2,y})} = \frac{\partial\left(\boldsymbol{\tau}_2^{\mathrm{ISP}}\right)_y}{\partial \dot{m}_{1,z}} = -\frac{\partial\left(\boldsymbol{\tau}_2^{\mathrm{ISP}}\right)_z}{\partial \dot{m}_{1,y}} = G'\alpha', \tag{A7}$$

where

$$2G' = \Gamma_1\left(d_{\mathrm{N}}/2\right) - \Gamma_2\left(d_{\mathrm{N}}/2\right). \tag{A8}$$

We finally note that some of the coefficients are related:

$$\frac{G}{G'\alpha'} = \frac{1}{\hbar}\frac{2el_{\mathrm{sf}}}{\sigma}\tanh(d_{\mathrm{N}}/2l_{\mathrm{sf}}). \tag{A9}$$

[1] A. Brataas, A. D. Kent, and H. Ohno, Nat. Mater. **11**, 372 (2012).
[2] H. Nakayama, M. Althammer, Y.-T. Chen, K. Uchida, Y. Kajiwara, D. Kikuchi, T. Ohtani, S. Geprägs, M. Opel, S. Takahashi, R. Gross, G. E. W. Bauer, S. T. B. Goennenwein, and E. Saitoh, Phys. Rev. Lett. **110**, 206601 (2013).
[3] Y. Kajiwara, K. Harii, S. Takahashi, J. Ohe, K. Uchida, M. Mizuguchi, H. Umezawa, H. Kawai, K. Ando, K. Takanashi, S. Maekawa, and E. Saitoh, Nature (London) **464**, 262 (2010).
[4] C. W. Sandweg, Y. Kajiwara, K. Ando, E. Saitoh, and B. Hillebrands, Appl. Phys. Lett. **97**, 252504 (2010).

[5] C. W. Sandweg, Y. Kajiwara, A. V. Chumak, A. A. Serga, V. I. Vasyuchka, M. B. Jungfleisch, E. Saitoh, and B. Hillebrands, Phys. Rev. Lett. **106**, 216601 (2011).
[6] L. H. Vilela-Leao, C. Salvador, A. Azevedo, and S. M. Rezende, Appl. Phys. Lett. **99**, 102505 (2011).
[7] C. Burrowes, B. Heinrich, B. Kardasz, E. A. Montoya, E. Girt, Y. Sun, Y.-Y. Song, and M. Wu, Appl. Phys. Lett. **100**, 092403 (2012).
[8] S. M. Rezende, R. L. Rodriguez-Suarez, M. M. Soares, L. H. Vilela-Leao, D. Ley Dominguez, and A. Azevedo, Appl. Phys. Lett. **102**, 012402 (2013).
[9] J. Xiao, G. E. W. Bauer, K.-C. Uchida, E. Saitoh, and S. Maekawa, Phys. Rev. B **81**, 214418 (2010).
[10] Y.-T. Chen, S. Takahashi, H. Nakayama, M. Althammer, S. T. B. Goennenwein, E. Saitoh, and G. E. W. Bauer, Phys. Rev. B **87**, 144411 (2013).
[11] J. C. Slonczewski, Phys. Rev. B **82**, 054403 (2010).
[12] J. Xingtao, L. Kai, K. Xia, and G. E. W. Bauer, Europhys. Lett. **96**, 17005 (2011).
[13] A. Kapelrud and A. Brataas, Phys. Rev. Lett. **111**, 097602 (2013).
[14] Y. Zhou, H. J. Jiao, Y. T. Chen, G. E. W. Bauer, and J. Xiao, Phys. Rev. B **88**, 184403 (2013).
[15] J. Xiao and G. E. W. Bauer, Phys. Rev. Lett. **108**, 217204 (2012).
[16] Y. Tserkovnyak, A. Brataas, G. E. W. Bauer, and B. I. Halperin, Rev. Mod. Phys. **77**, 1375 (2005).
[17] P. Grünberg, R. Schreiber, Y. Pang, M. B. Brodsky, and H. Sowers, Phys. Rev. Lett. **57**, 2442 (1986)
[18] B. Heinrich, Y. Tserkovnyak, G. Woltersdorf, A. Brataas, R. Urban, and G. E. W. Bauer, Phys. Rev. Lett. **90**, 187601 (2003).
[19] Z. Q. Qiu, J. Pearson, and S. D. Bader, Phys. Rev. B **46**, 8659 (1992).
[20] M. B. Jungfleisch, V. Lauer, R. Neb, A. V. Chumak, and B. Hillebrands, Appl. Phys. Lett. **103**, 022411 (2013).
[21] R. A. Serway, in *Principles of Physics*, 2nd ed. (Saunders College Pub., Texas, London, 1998), p. 602.
[22] A. A. Serga, A. V. Chumak, and B. Hillebrands, J. Phys. D: Appl. Phys. **43**, 264002 (2010).
[23] H. Skarsvåg, A. Kapelrud, and A. Brataas, arXiv:1407.0635.
[24] V. E. Demidov, S. Urazhdin, E. R. J. Edwards, M. D. Stiles, R. D. McMichael, and S. O. Demokritov, Phys. Rev. Lett. **107**, 107204 (2011).
[25] S. S.-L. Zhang and S. Zhang, Phys. Rev. Lett. **109**, 096603 (2012).
[26] C. Hahn, G. de Loubens, O. Klein, M. Viret, V. V. Naletov, and J. Ben Youssef, Phys. Rev. B **87**, 174417 (2013).